

N92-14349

THE EFFECTS OF MANUFACTURING TOLERANCES ON THE VIBRATION OF
AERO-ENGINE ROTOR-DAMPER ASSEMBLIES*

J.E.H. Sykes and R. Holmes
Department of Mechanical Engineering
University of Southampton
Southampton, England

A range of rotor assemblies incorporating one and two squeeze-film dampers with various static misalignments is investigated. Waterfall diagrams are constructed which demonstrate the effects of such misalignment and damper support flexibility on the nature and severity of subsynchronous resonance and jump phenomena. Vibration signatures of similar rotor-bearing assemblies are shown to contrast strongly due to different accumulations of tolerances during manufacture, fitting and operation.

*Carried out under a grant funded by The Science and Engineering Research Council, UK and Rolls Royce plc.

Notation

<u>Notation</u>	<u>Description</u>	<u>Unit</u>
A_1	SFD1 Bearing Factor, $\pi \cdot \mu \cdot R_1 (l_1/c_1)^3 f^2 / b J(k_2 \cdot l)$	-
A_2	SFD2 Bearing Factor, $\pi \cdot \mu \cdot R_2 (l_2/c_2)^3 b / J(k_2 \cdot l)$	-
a, b	Rig Dimensions	m
c	SFD Radial Clearance	m
d	Rig Dimension	m
e	SFD Eccentricity	m
E_0	SFD Static Eccentricity Ratio	-
f	Rig Dimension	m
G	SFD Groove Depth	m
G_w	SFD Groove Width	m
I	Rotor Moment of Inertia per land	kg.m ²
k	Flexible Bearing Support Stiffness per land	N/m
k_1	Non-Dimensional Stiffness per land, $k_1 \cdot f^2 / (l \cdot w^2)$	-
k_2	Non-Dimensional Stiffness per land, $k_2 \cdot b^2 / (l \cdot w^2) = (w/w_n)^{-2}$	-
l	SFD Land Width	m
N	Number of Lands per SFD	-
P_1	SFD Radial Film Force per land	N
P_2	SFD Tangential Film Force per land	N
P_c	Rotor Mass Unbalance Force per land	N
P_{sup}	SFD Oil Supply Pressure	N/m ² , psi
Q_{c2}	Non-Dimensional Unbalance Force, $P_c \cdot a \cdot b / (l \cdot c_2 \cdot w^2)$	-
Q_s	Non-Dimensional Static Force, $m \cdot g \cdot d \cdot b / (l \cdot c_2 \cdot w^2)$	-
R	SFD Mean Radius	m
t	Time	s
w	Rotor Rotational Speed	rad/s
w_n	Rotor-Bearing Assembly First Bounce Vibration Mode Frequency (Configurations 1a,b)	rad/s
Z	Dummy parameter	-
α	SFD Journal Attitude Angle	rad
δ	SFD1 non-dimensional preload (gravity offset), $\{[m \cdot g \cdot d / (b \cdot k_2)] + c_2\} \cdot f / (b \cdot c_1)$	-
E	Eccentricity Ratio, e/c	-
μ	Oil Dynamic Viscosity	Ns/m ²
\cdot	Derivative with respect to time, t	1/s
$'$	Derivative with respect to Non-Dimensional Time, $w \cdot t$	1/rad
$-$	Non-Dimensional Quantity	
$_1$	After a parameter denotes SFD1	
$_2$	After a parameter denotes SFD2	

Abbreviations

<u>Abbreviation</u>	<u>Description</u>
c/min	Cycles Per Minute
EO	Engine Order
DOF	Degree(s) of Freedom
FFT	Fast Fourier Transform
RRG	Rotor Relative to Ground
SERC	Science & Engineering Research Council
SFD	Squeeze-Film Damper

INTRODUCTION

The major source of aero-engine rotor vibration is the state of rotor balance which can alter progressively during service and sharply as a result of minor damage. Even with well balanced rotors sudden unexpected non-linear vibration phenomena, such as jumps and subharmonic resonances, can occur. The most prolific sources of non-linearity are the squeeze-film dampers which surround some of the bearings.

The squeeze-film damper, SFD has been applied in a wide range of rotor-bearing assemblies to attenuate resonant vibration and to combat rotor instability. The ever increasing demand for high performance indicates that rotor vibration isolation utilising squeeze-film dampers will remain a prominent feature of future turbomachinery designs.

SFD response characteristics and non-linear jump phenomena have been demonstrated by numerous workers. White (Ref 1) cited jumps in a vertical rotor rig and Simandiri et al (Ref 2) studied jumps on an idealised, horizontal rotor, single SFD rig, aligned to exhibit synchronous circular orbits. Holmes et al (Ref 3) obtained jump phenomena with a horizontal rotor rig involving a rigidly housed SFD, carrying appreciable rotor weight. Actual engine tests have demonstrated jump phenomena, such as observed by Gunter et al (Ref 4).

The operation of a SFD is least beneficial when subharmonic resonances, sometimes dominating the synchronous response, develop in conditions of light damping. Subharmonics of orders up to four were cited by Nikolajsen et al (Ref 5) from a flexible rotor rig. Gunter et al (Ref 4) carried out numerical time marching to observe the transient analysis of a rotor which indicated some half engine order subharmonic resonance in its SFD orbits.

The explanation of such jump phenomena and subharmonic resonances observed in engines employing multiple shaft, multiple SFD assemblies is difficult. Previous simulation of such phenomena on simplified test rigs has met with limited success. Consequently, existing literature has failed to address this problem comprehensively. Appreciation of the relationship between the basic components of assemblies and their potential for introducing misalignment between SFDs provides an insight into the complex responses observed in practice.

THE TEST FACILITY

Aero-engine rotor operating speeds are often above one or more rigid body modes and below any significant flexural mode. Because of this damping can be successfully introduced in the bearing supports to attenuate vibration induced by unbalance.

To create a realistic configuration a three-bearing rigid rotor assembly incorporating the essential features of a small aero-engine was utilised, Fig 1. This test rig was used to investigate the operation of the SFD's, 1, at two of its three rolling-element bearings, 2. The self alignment capability of the bearing, 3, constituted a pivot about which an antisymmetric, or conical mode of vibration occurred when the rotor, 4, was acted upon by a force arising from rotation of the unbalance mass, 5.

Flexible bars, 6, simulated pedestal flexibility and were mounted into heavy foundation blocks, 7, which represented ground. Comparisons between different rig configurations (Table 1) allowed the influence of individual assembly components and in-service assembly misalignment conditions to be analysed. Fig 2 gives a schematic diagram of a SFD and relevant dimensions are given in Appendix 1.

Tests were carried out employing four unbalance masses. Values of the unbalance parameter, Q_{c2} , ranged from 0.245 to 0.733, or 25g to 75g mass, respectively and rotor speed from 900 to 4860 c/min. Oil supply pressures were varied between 2 psi and 24 psi when one SFD was active and up to 15 psi with two SFDs active. The tests were analysed by studying the SFD orbit magnitudes and the phase angles between SFD eccentricity vectors and the unbalance. The rotor speed was represented as a frequency ratio, by dividing by the first bounce mode frequency of configuration 1a (Table 1), namely 32.4 Hz. Rotor displacements relative to ground and relative to the SFD2 housing were sampled by a spectrum analyser, utilising the Hanning time window.

The transient response of the rig, when stationary, to impulses from a soft hammer enabled its static natural frequencies to be determined.

Responses for configurations 1a through to 2b demonstrated a lowest natural frequency at 32.4 Hz, in both the horizontal (x) and the vertical (y) directions. Higher natural frequencies were 200 Hz or more. Configurations 3a and 3b gave a lowest natural frequency at 34.8 Hz in the x direction and 36.8 Hz in the y direction, indicating a degree of anisotropy.

THEORETICAL CONSIDERATIONS

The theoretical analysis assumed the following;

1. The Reynolds Equation and the Short Bearing approximation apply.
2. The rotor remains rigid.
3. The flexible bars contribute a constant, linear radial stiffness to the system.

The rotor-bearing assembly was modelled as a dynamic system, Fig 3, with the relevant equations summarised in Appendix 2.

Simpson's numerical integration procedure was employed to derive film force predictions at each step of a Runge-Kutta computation scheme. Following work by Feng and Hahn (Ref 6) a cavitation pressure, P_{min} of absolute zero (-14.7 psi gauge) was adopted.

The results of prime interest were the displacement orbit size and phase with respect to unbalance, to be compared with the experimentally observed rig behaviour.

Software development provided waterfall diagrams and, with a frequency resolution of 1.0 Hz, have provided sufficient spectral information at reasonable mainframe speeds and data storage requirements. Attention was given to the case with unbalance, Q_{c2} equal to 0.611 as this illustrated all the non-linear phenomena encountered during testing.

TABLE 1 Test Rig Configurations

Test Rig Configuration	Static Set Up		Simple Representative Rig Diagram
	E_{01}	E_{02}	
1a	0.0	-	
1b	0.4, 0.8	-	
2a	0.0, 0.5	1.0	
2b	1.0	0.0	
3a	1.0	1.0	
3b	0.0	1.0	

EXPERIMENTAL & THEORETICAL RESULTS

The motion of the rotor in configuration 1a was 'well behaved' for reasonably low unbalance factors (Fig 4a), being attenuated by the damper action of SFD1. When the unbalance factor was above a certain level then SFD1, even with increased supply pressure, had difficulty in maintaining an acceptable, damped response and jump phenomena became a feature. This response could take the form of a high vibration level persisting through unity frequency ratio without any jump down. Alternatively, the high response could be abruptly reduced by a jump down to some lower vibration level. Increasing oil pressure reduced the peak eccentricity and the size of the accompanying phase jump to some degree. The orbits were almost circular in shape.

At speeds higher than the minimum jump frequency, any persistently large rotor excursions were quite stable and an impact delivered to the rotor by a soft hammer could not induce a jump down. After inversion at high speed, subsynchronous response occurred at a frequency equal to the natural frequency, Fig 5a. All of the above observations were supported by theoretical predictions (Fig 4b and Fig 5b).

With rig configuration 1b the effect of increasing the static eccentricity, E_{01} , in SFD1 was to generally increase the damping. For E_{01} 0.8 configuration 1b produced a jump down with increasing speed when the unbalance factor, Q_{02} , was only 0.490 (Fig 6a) and strong subharmonic resonance developed at the higher speeds. This is clearly demonstrated in the bottom right experimental orbit ($w/w_n = 2.253$) of Fig 6c. Again

theoretical predictions supported the experimental findings (Figs 6b and 6d).

The experimental results for configuration 2a showed that the rig response was acceptably low for reasonably small unbalance factors, being attenuated by the damper actions of SFD1 and SFD2. Increasing oil pressure required an increase in the unbalance at which bistable operation occurred, introducing jumps. Subsynchronous activity persisted at speeds above twice the first bounce mode frequency (Fig 7a), and higher order vibrations were present over most of the speed range. Again theoretical predictions (Fig 7b) supported the experimental results.

The effect of introducing a static eccentricity, E_0 , of 0.5, to configuration 2a was to change the experimental jump characteristics and the nonsynchronous frequency response, Fig 8a. A jump up and a jump down were observed above the first bounce mode frequency. Half engine orders of large amplitude were present at rotor speeds around 2.5 times the first non-rotating bounce frequency. Theoretical predictions (Fig 8b) again show good agreement.

Experimental results revealed that the change in static misalignment conditions from configuration 2a, constituting configuration 2b, removed the high synchronous amplitudes associated with the first bounce frequency, leaving an apparently well damped response. However, with high unbalances and above the first bounce frequency, a sudden jump up in vibration amplitude with increasing speed was demonstrated, Fig 9a. This speed decreased as unbalance was increased. Corresponding theoretical results are given in Fig 9b.

The most significant result from configurations 3a and 3b was that rotor excursions were much larger than previously experienced, Fig 10. Jump phenomena were still in evidence but below the static natural frequency of the assembly. 'Safe' operation at speeds above the first bounce mode was achievable for all but the highest unbalance. The major effect of statically offloading, or centralising SFD1, configuration 3b, was to appreciably reduce the subsynchronous and higher engine order activity. Configuration 3a exhibited some significant $1/2$ EO at just higher than the jump speed. This subharmonic was absent from the corresponding response in configuration 3b.

NON-LINEAR PHENOMENA

The jump up with decreasing speed or jump down with increasing speed above the first bounce mode frequency corresponds to the classical non-linear 'hardening spring' response. The difference in the two speeds is the effective range of the bistable region. Equally, a jump up with increasing speed might be attributed to a non-linear 'softening spring' effect.

In addition there is experimental evidence (Ref 3) that sudden venting of the SFD from atmosphere changes the effective cavitation conditions, and could promote jump up. Oil-film pressure measurements taken for configuration 2b indicated that the minimum pressure rose after jump up on run up. A limited hysteresis in the rotor speeds, of about 4 Hz at most, was noted between the jump up on run up and the jump down on run down.

Subharmonic resonances of half engine order have been demonstrated both experimentally and theoretically. Non-synchronous activity at $3/2$ EO, $5/2$ EO and $7/2$ EO accompanied these subharmonics.

A statically centred SFD in configurations 1a and 2a gave rise to weak subsynchronous resonance at the static natural frequency, Figs 5 and 7. Static eccentricity applied to the same SFD increased its non-linearity and excited strong half engine order subharmonics, this time corresponding to the dynamic natural frequency, determined by the stiffnesses of both the static components and the SFD's, Figs 6 and 8.

PRACTICAL IMPLICATIONS ARISING FROM THE RESULTS

Jump phenomena can lead to high transmitted forces and sudden changes in engine vibration. Non-synchronous response causes fluctuating rotor stresses in flexible shafts. It also leads to subharmonic resonances, sometimes larger than the resonances developed by unbalance.

The present research has demonstrated the ability of a range of rotor-bearing assemblies, incorporating unsealed SFDs, to exhibit a number of undesirable non-linear phenomena.

Aero-engine rotor assemblies employ one or more SFD's per rotor, each within a bearing pedestal characterised by a certain stiffness. A degree of misalignment in three-bearing assemblies is inevitable due to the 'stack up' of tolerances and the effects of high speed manoeuvres of military aircraft may serve to further affect the bearing alignments.

Most assemblies employ sealed SFD's to improve damping capacity and strong jump phenomena are not always a problem. However, there have been many reported instances and results emanating from this research indicate the physical mechanisms which promote such phenomena.

Holmes and Dogan's work (Ref 3) indicated that a jump up on run up can exist when a rotor is supported by a rigidly housed SFD and high vibration amplitudes can prevent higher speeds being attained. The same SFD, when mounted flexibly can respond without a jump up but non-synchronous rotor centre orbits can be introduced at speeds around the assembly's natural frequency. Low vibration levels can, however, be achieved at speeds above the natural frequency.

Based on the present research, assemblies with a single SFD, centred by a flexible rotor support, are likely to exhibit jumps only when the unbalance is relatively high, probably outside acceptable contractual limits. These jumps are analogous to the classical non-linear hardening spring response and arise from the stiffness property of a cavitated squeeze-film which increases with speed. On the other hand, the same assemblies with the SFD statically off-centred are likely to demonstrate that low unbalance, possibly within contractual limits, can excite jumps and strong subharmonic resonance.

Some assemblies incorporate two SFD's with very different housing supports, for example, one rigidly housed and the other flexibly housed. With the former statically centred and the latter carrying the rotor weight the

response might well be governed by the former, the latter having little influence. Jump phenomena will occur around the first bounce mode frequency. At high speed, after jump down, satisfactory operation should be possible with low amplitude subsynchronous activity at the bounce mode frequency. Raising the housing of the rigidly-supported SFD will result in subharmonic resonance possibly dominating the synchronous response and degrading the vibration performance within the operating range.

By raising the rigidly mounted SFD housing further still, until it carries the static rotor weight and such that the flexibly supported SFD is centred, safe operation can only be guaranteed up to a certain speed, at which a strong jump up can be expected. On running down, the vibration will jump down at a lower speed. A static eccentricity applied to the flexibly-supported SFD may alleviate the jump or increase the speed at which it takes place due to some of the rotor weight being supported dynamically by this flexibly supported SFD.

The flexible supporting of both SFDs with similar support stiffnesses should give rise to desirable operation for all but a small speed range around the first bounce mode. It may be that jumps and subharmonic resonance at these speeds could be eliminated by additional damping from SFD sealing without degrading the performance within the rest of the speed range. Centralising one of the SFDs has the effect of reducing the subharmonic resonance at speeds around the first bounce mode.

The presence of half engine order subharmonic resonance dominating the synchronous response at speeds well above the bounce frequency would suggest that one of the SFDs was not supported flexibly enough and was neither fully eccentric, nor concentric in its housing. If, in another case, strong jumps up on acceleration were encountered at speeds well above the bounce mode, then it might be caused by a SFD housing support being too rigid for it to safely carry the rotor weight. Improvements might be achieved by off-loading the 'rigidly' housed SFD, softening its support or both.

CONCLUSIONS

The rig configurations have demonstrated a range of non-linear responses associated with aero-engine rotor-bearing assemblies and there is pleasing similarity between the experimental and theoretical responses. The experimental dependence of jump phenomena and subharmonic resonances upon SFD misalignment and housing support has been clearly illustrated in the theoretical results.

This work has provided an insight into the mechanism of SFD phenomena and the practical implications arising from these findings should be useful in the design of rotor-bearing assemblies.

REFERENCES

1. WHITE D.C., Squeeze Film Journal Bearings, PhD Thesis, University of Cambridge, 1970.
2. SIMANDIRI S. & HAHN E.J., Experimental Evaluation of the Predicted

- Behaviour of Squeeze-Film-Bearing-Supported Rigid Rotors, IMechE, J Mech Eng Science, Feb 1976, pp 109-117.
3. HOLMES, R. & DOGAN M., Investigation of a Rotor Bearing Assembly Incorporating a Squeeze-Film Damper Bearing, IMechE, J Mech Eng Science, 1982, Vol 24, No 3, pp 129-137.
 4. GUNTER E.J., BARRETT L.E. & ALLAIRE P.E., Design of Nonlinear Squeeze-Film Dampers for Aircraft Engines, Trans ASME, J Lubric Technology, 1977, pp 57-64.
 5. NIKOLAJSSEN J.L. & HOLMES R., Investigation of Squeeze-Film Isolators for the Vibration Control of a Flexible Rotor, IMechE, J Mech Eng Science, 1979, Vol 21, No 4, pp 247-252.
 6. FENG N.S. & HAHN E.J., Effects of Gas Entrainment on Squeeze Film Damper Performance, Trans ASME, J Tribology, 1987, Vol 109, pp 149-154.

APPENDICES

APPENDIX 1 SFD Geometry & Other Rig Parameters

SFD1 Damper Geometry

c_1	= 0.000254 (m)	$(1/c)_1$	= 44.2 (-)
$(1/R)_1$	= 0.144 (-)	G_1	= 0.002 (m)
Gw_1	= 0.004 (m)	N_1	= 2 (-)

SFD2 Damper Geometry

c_2	= 0.000216 (m)	$(1/c)_2$	= 41.6 (-)
$(1/R)_2$	= 0.132 (m)	G_2	= 0.002 (m)
Gw_2	= 0.004 (m)	N_2	= 2 (-)

Rig Parameters

a	= 1.019 (m)	b	= 0.9716 (m)
d	= 0.5434 (m)	f	= 0.5968 (m)
l	= 11.5 (kg.m ² per land)	k_1	= 0.505 (MN/m per land)
k_2	= 0.505 (MN/m per land)	w_n	= 203.58 (rad/s)
μ	= 6.0 (cP average)		

APPENDIX 2 Equations of Motion

Equations of motion can be developed by taking moments about the pivot bearing, referring to Figs 3a,b and c. Equations describing the rotor motion at the SFD2 journal in a cartesian (x,y) coordinate system can be written, non-dimensionally, as

Configurations 1a,b (Table 1)

$$\begin{aligned}
 y_2'' &= Q_{c_2} \cdot \sin(w.t) - (\bar{k}_2 \cdot E_1 \cdot \sin(\alpha_1)) (c_1/c_2) (b/f) \\
 &\quad - (c_1/c_2) (b/f) (\bar{P}_{1,1} \cdot \sin(\alpha_1) + \bar{P}_{2,1} \cdot \cos(\alpha_1)) - Q_s \\
 x_2'' &= Q_{c_2} \cdot \cos(w.t) - (\bar{k}_2 \cdot E_1 \cdot \cos(\alpha_1)) (c_1/c_2) (b/f) \\
 &\quad - (c_1/c_2) (b/f) (\bar{P}_{1,1} \cdot \cos(\alpha_1) - \bar{P}_{2,1} \cdot \sin(\alpha_1))
 \end{aligned}$$

Configurations 2a,b and 3a,b

$$y_2'' = Q_{c2} \cdot \sin(w.t) - (\bar{P}_{12} \cdot \sin(\alpha_2) + \bar{P}_{22} \cdot \cos(\alpha_2)) \\ - (c_1/c_2)(b/f)(\bar{P}_{11} \cdot \sin(\alpha_1) + \bar{P}_{21} \cdot \cos(\alpha_1)) - Q_s$$

$$x_2'' = Q_{c2} \cdot \cos(w.t) - (\bar{P}_{12} \cdot \cos(\alpha_2) - \bar{P}_{22} \cdot \sin(\alpha_2)) \\ - (c_1/c_2)(b/f)(\bar{P}_{11} \cdot \cos(\alpha_1) - \bar{P}_{21} \cdot \sin(\alpha_1))$$

where $\bar{P}_{1,2_2} = P_{1,2_2} \cdot b^2 / (I \cdot c_2 \cdot w^2)$

$$\bar{P}_{1,2_1} = P_{1,2_1} \cdot f^2 / (I \cdot c_1 \cdot w^2)$$

and $y_2'', x_2'' = y_2, x_2 / (c_2 \cdot w^2)$

Variation in the SFD static misalignment conditions is achieved by employing the term δ . Thus, converting the cartesian rotor motion at SFD2 relative to ground to the SFD1 polar motion for configurations 2a and 2b;

where $Z = (f \cdot c_2 / b \cdot c_1)$

$$E_{y_1} = Z \cdot \bar{y}_2 - E_{s1} + \delta \quad E_{y_1}' = Z \cdot y_2'$$

$$E_{x_1} = Z \cdot \bar{x}_2 \quad E_{x_1}' = Z \cdot x_2'$$

$$E_1 = (E_{x_1}^2 + E_{y_1}^2)^{1/2}$$

$$\alpha_1 = \arctan(E_{y_1} / E_{x_1})$$

$$E_1' = (E_{x_1} \cdot E_{x_1}' + E_{y_1} \cdot E_{y_1}') / E_1$$

$$\alpha_1' = (E_{x_1} \cdot E_{y_1}' - E_{y_1} \cdot E_{x_1}') / E_1^2$$

It has been shown (Ref 3) that the SFD housing mass of the test facility for a series SFD and spring configuration has little influence on the rotor dynamics. Thus, neglecting the SFD2 housing mass the force prevailing in the spring, k_2 must equal and oppose the resultant SFD2 film force. Therefore, we can conclude that, for Configurations 2a,b and 3a,b,

$$\bar{k}_2 (\bar{y}_2 - E_2 \cdot \sin(\alpha_2)) = \bar{P}_{12} \cdot \sin(\alpha_2) + \bar{P}_{22} \cdot \cos(\alpha_2)$$

$$\bar{k}_2 (\bar{x}_2 - E_2 \cdot \cos(\alpha_2)) = \bar{P}_{12} \cdot \cos(\alpha_2) - \bar{P}_{22} \cdot \sin(\alpha_2)$$

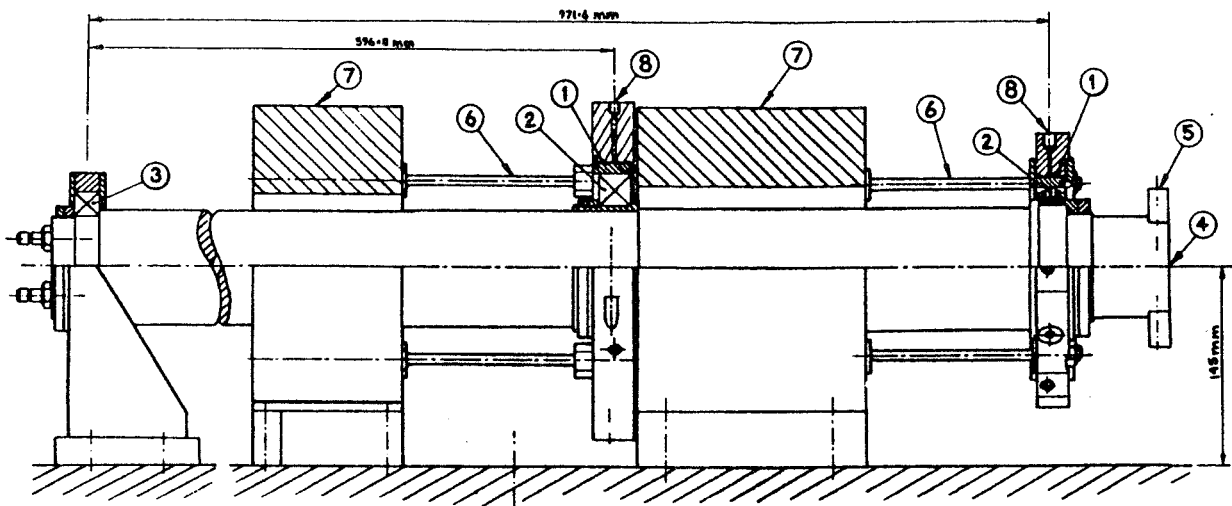
and, similarly, for Configurations 3a,b only,

$$\bar{k}_1 (\bar{y}_1 - E_1 \cdot \sin(\alpha_1)) = \bar{P}_{11} \cdot \sin(\alpha_1) + \bar{P}_{21} \cdot \cos(\alpha_1)$$

$$\bar{k}_1 (\bar{x}_1 - E_1 \cdot \cos(\alpha_1)) = \bar{P}_{11} \cdot \cos(\alpha_1) - \bar{P}_{21} \cdot \sin(\alpha_1)$$

where $\bar{x}_1 = \bar{x}_2 (c_2/c_1)(f/b)$

$$\bar{y}_1 = \bar{y}_2 (c_2/c_1)(f/b)$$



- | | | | |
|---|-------------------------|---|------------------|
| 1 | Squeeze-Film Damper | 5 | Unbalance Mass |
| 2 | Rolling Element Bearing | 6 | Flexible Bar |
| 3 | Self Aligning Bearing | 7 | Foundation Block |
| 4 | Rotor | 8 | Oil Supply Port |

Fig 1 Details of Fully Assembled Experimental Rig

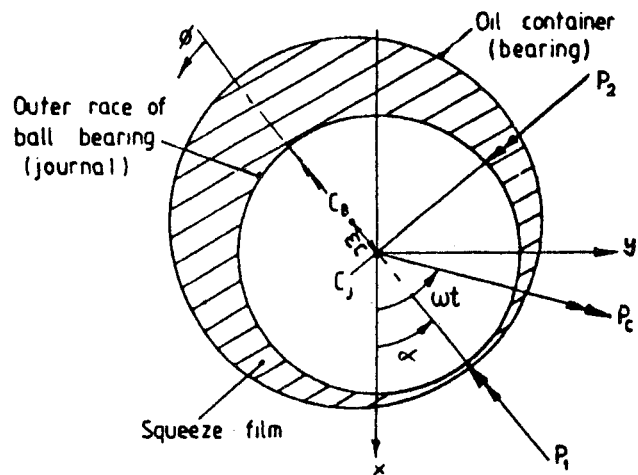
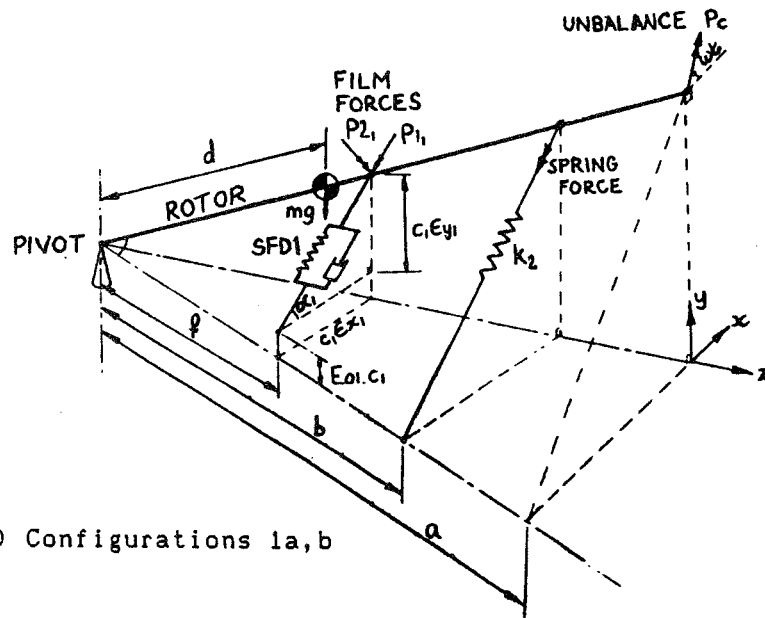
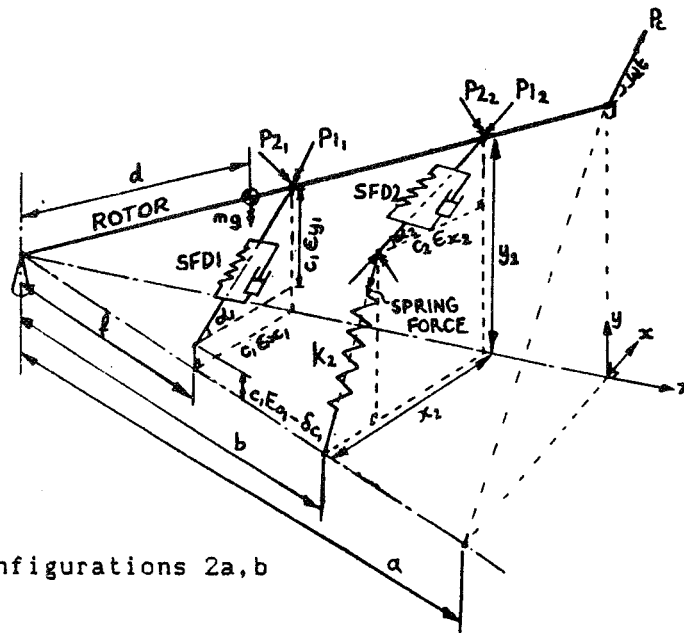


Fig 2 The Squeeze-Film Damper



(a) Configurations 1a, b



(b) Configurations 2a, b

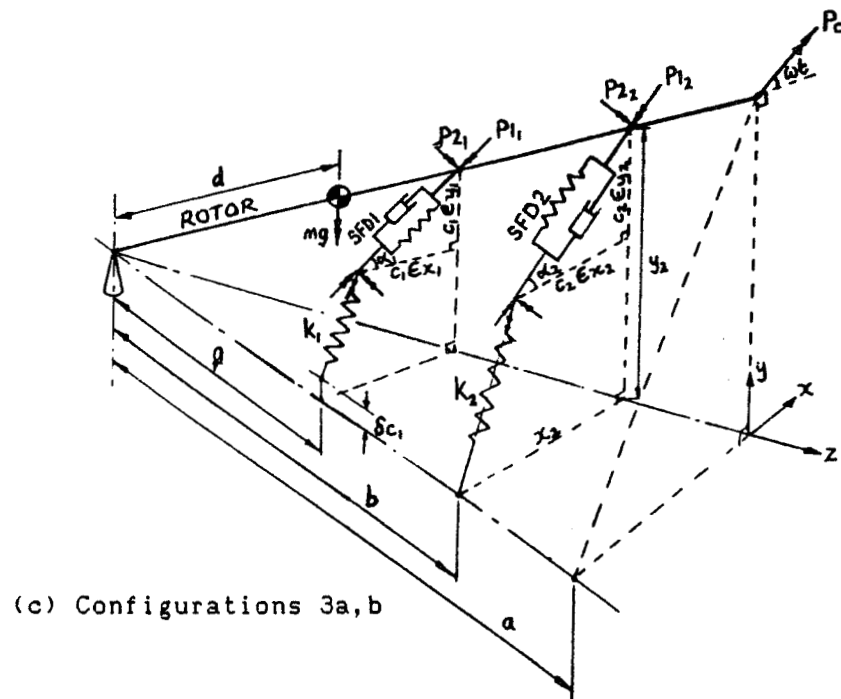


Fig 3 Rig Model Diagrams

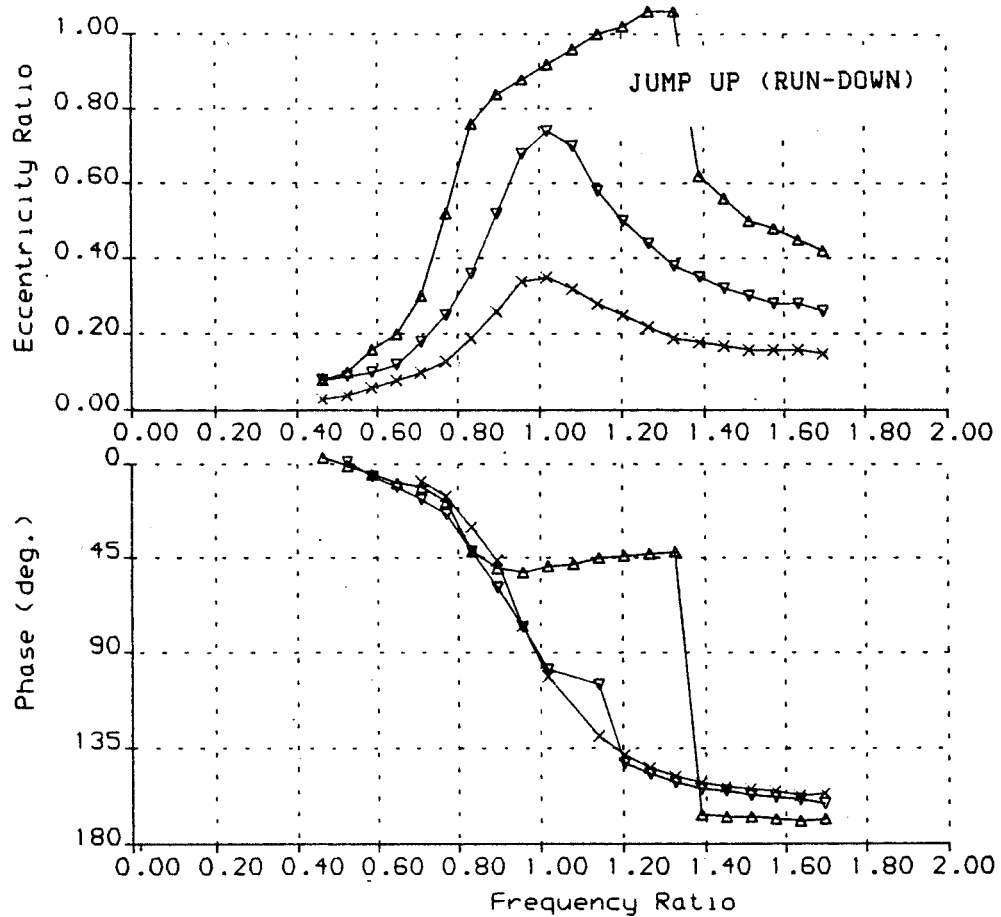
Fig 4a

SQUEEZE-FILM DAMPER SFD1 (0.5mm Groove Depth)

EXPERIMENTAL RESULTS

	Δ	∇	\times
A =	0.2132E -1	0.2132E -1	0.2132E -1
Qc2=	0.7332E 0	0.4901E 0	0.2450E 0
Eo =	0.0000E 0	0.0000E 0	0.0000E 0
Psup=	0.2000E 1	0.2000E 1	0.2000E 1

(ps1)



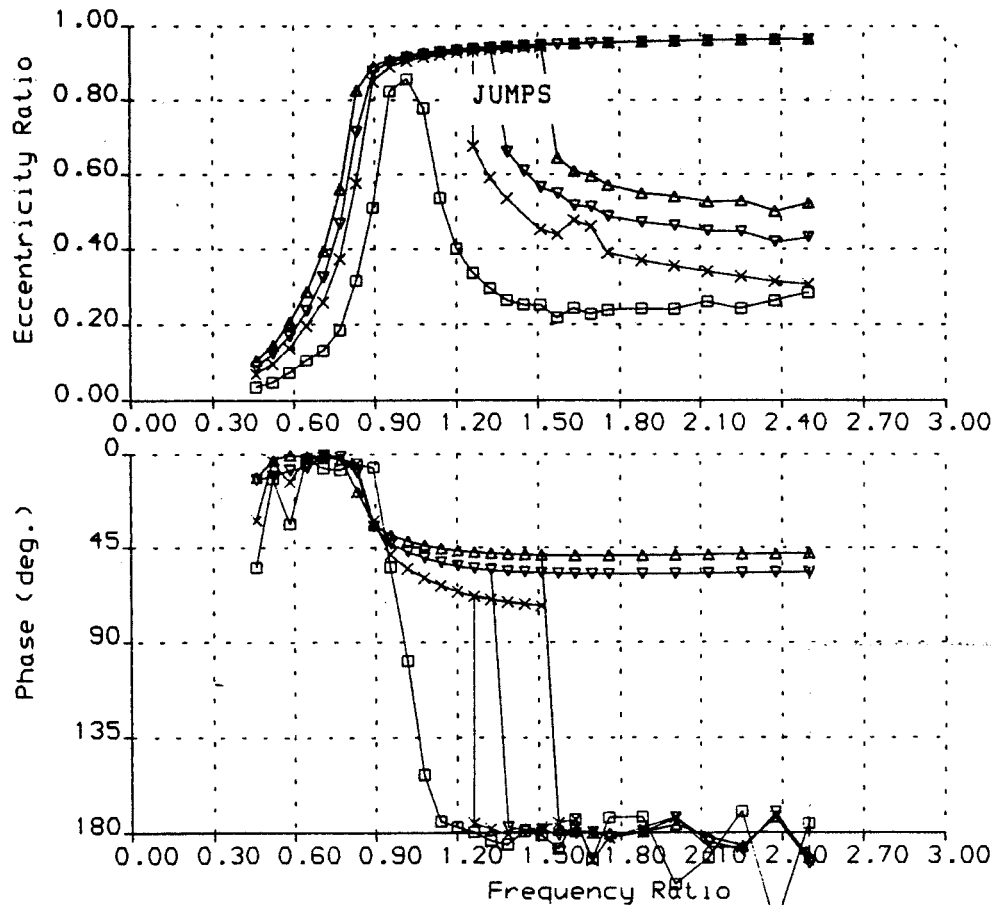
ROTOR-BEARING ASSEMBLY RESPONSE TO UNBALANCE
SQUEEZE-FILM DAMPER RESEARCH Rig ConFig. 1a

Fig 4b

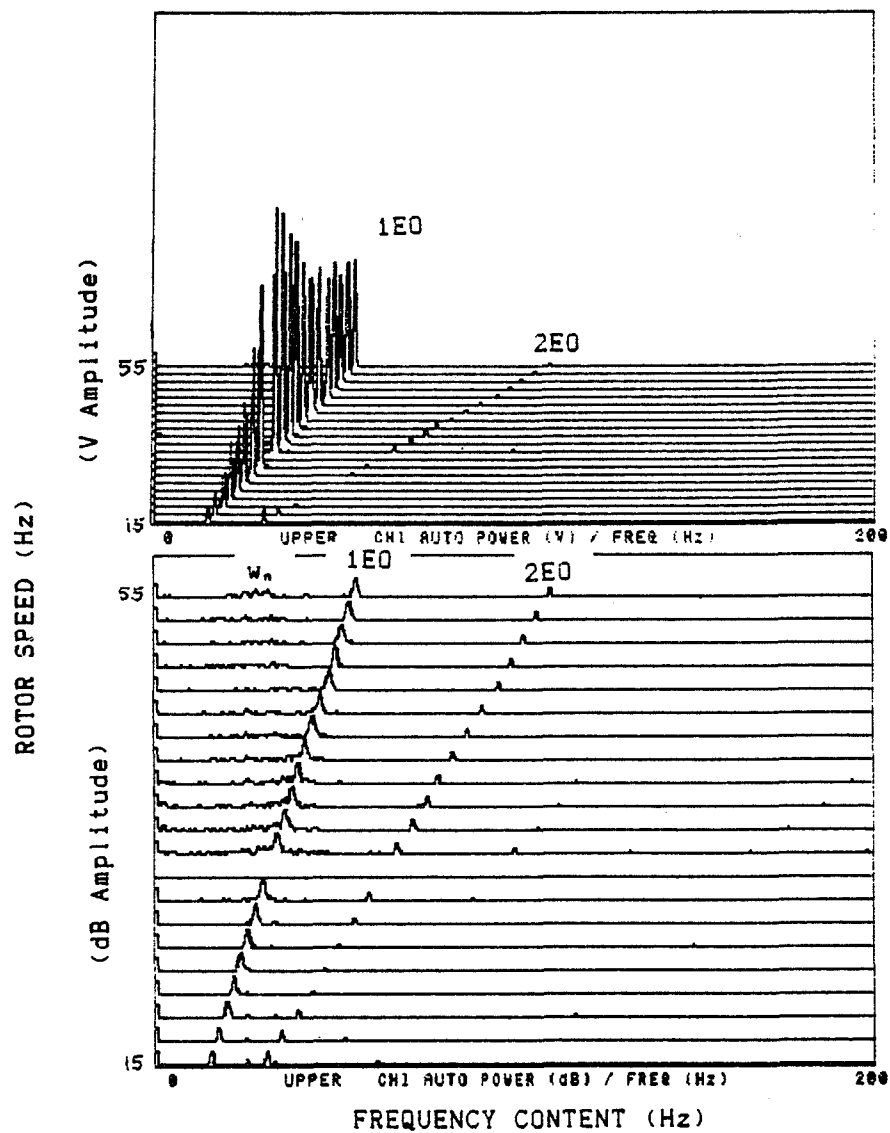
SQUEEZE-FILM DAMPER SFD1

THEORETICAL NUMERICAL SOLUTION

	Δ	∇	\times	\square	
A =	0.2132E -1	0.2132E -1	0.2132E -1	0.2132E -1	
Qc2=	0.7332E 0	0.6107E 0	0.4901E 0	0.2450E 0	
Eo =	0.0000E 0	0.0000E 0	0.0000E 0	0.0000E 0	
Psup=	0.2000E 1	0.2000E 1	0.2000E 1	0.2000E 1	(psi
Pmin=	-.1470E 2	-.1470E 2	-.1470E 2	-.1470E 2	(psi



ROTOR-BEARING ASSEMBLY RESPONSE TO UNBALANCE
 SQUEEZE-FILM DAMPER RESEARCH Rlg Config. 1a



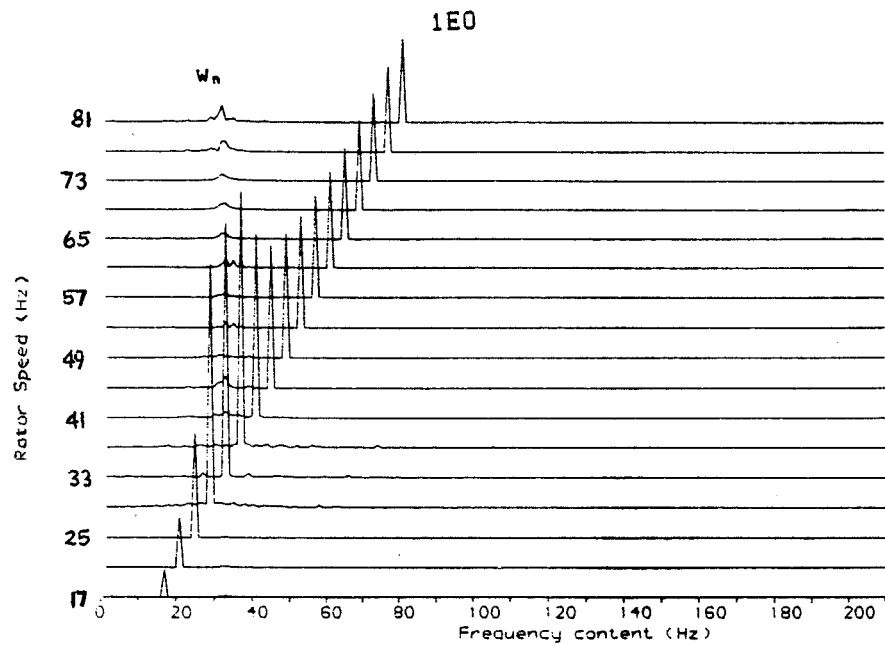
Experimental Waterfall Diagram

(a)

Configuration 1a ($Q_{c2}=0.490$, $P_{sup}=2\text{psi}$)

Fig 5

$A = 0.213200E -1$
 $Qc2 = 0.490097E 0$
 $Eo = 0.000000E 0$
 $Psup = 0.200000E 1 \text{ (psi)}$
 $Pmin = -0.147000E 2 \text{ (psi)}$

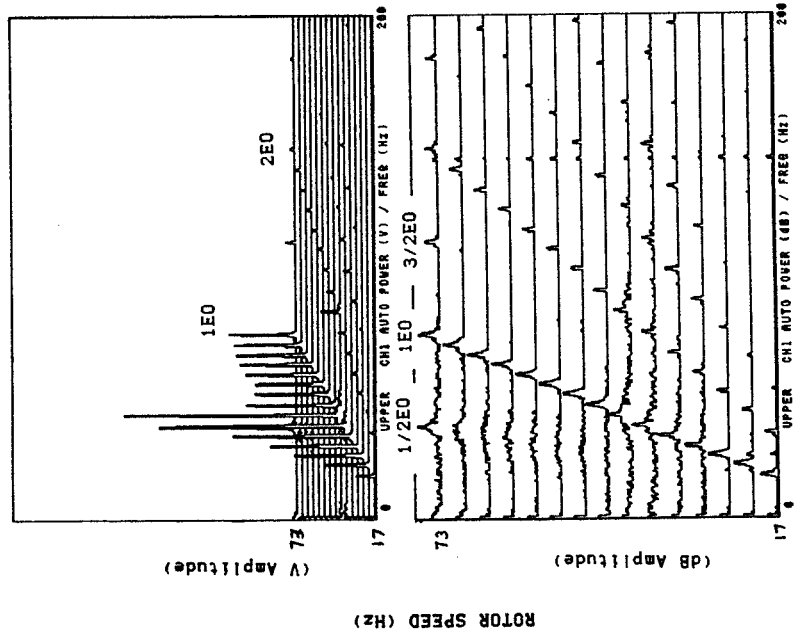


PREDICTED WATERFALL DIAGRAM
 SQUEEZE-FILM DAMPER RESEARCH: Rotor-Bearing Response

(Linear Amplitude)

Theoretical Waterfall Diagram

(b)



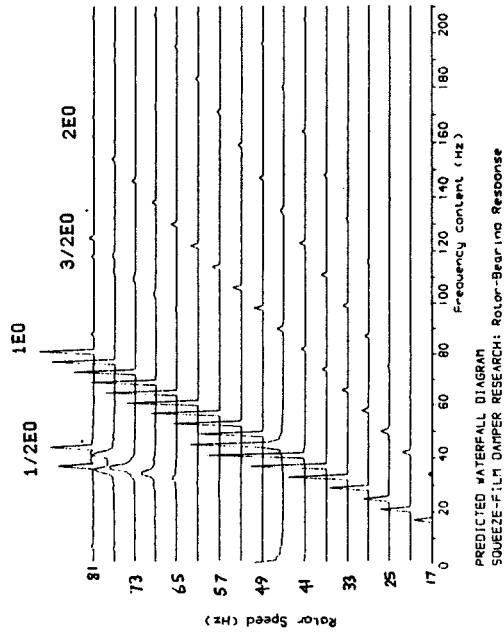
Experimental Waterfall Diagram

(a)

Configuration 1b ($\alpha_2=0.490$, $P_{sup}=2\text{psi}$, $E_1=0.8$)

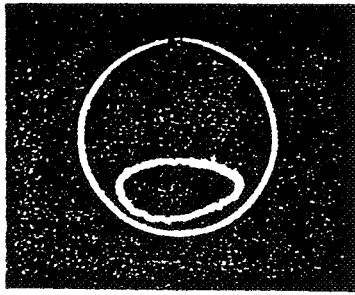
Fig 6

$A = 0.213200E -1$
 $Qc2 = 0.49097E 0$
 $E_0 = 0.803000E 0$
 $P_{sup} = 0.200000E 1 (\text{psi})$
 $P_{m,n} = -0.147000E 2 (\text{psi})$

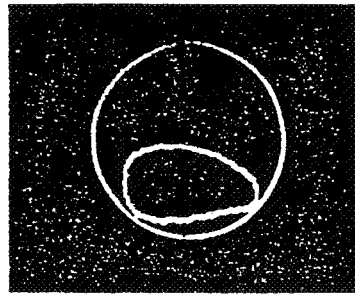


Theoretical Waterfall Diagram

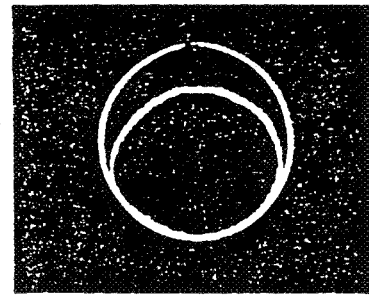
(b)



29 Hz ($W/W_n = 0.895$)

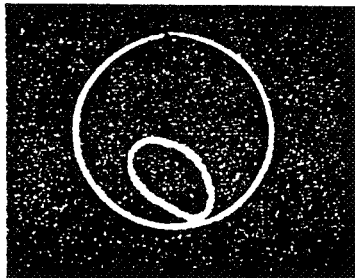


33 Hz ($W/W_n = 1.019$)

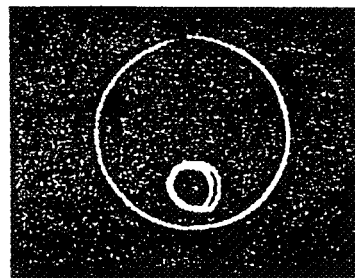


41 Hz ($W/W_n = 1.265$)

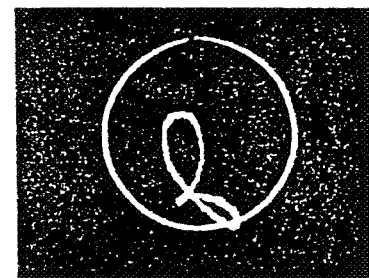
ROTOR SPEED



43 Hz ($W/W_n = 1.327$)

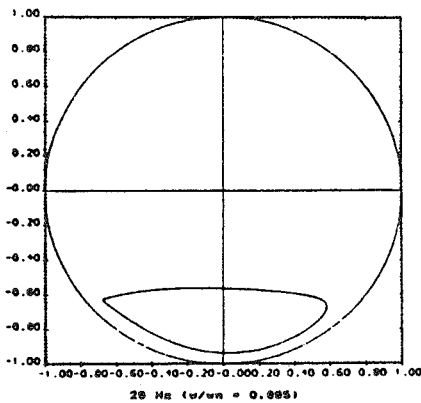


65 Hz ($W/W_n = 2.006$)

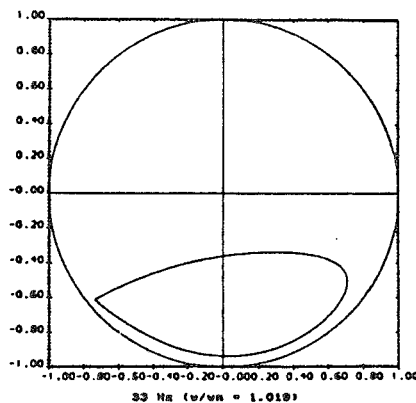


73 Hz ($W/W_n = 2.253$)

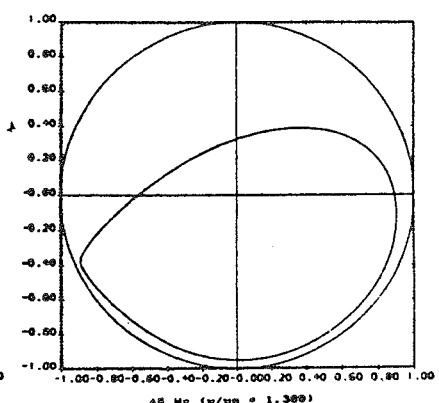
(c) SFD1 EXPERIMENTAL ORBITS (Configuration 1b, $Q_{c2} = 0.490$, $P_{sup} = 2\text{psi}$, $E_{o1} = 0.8$)



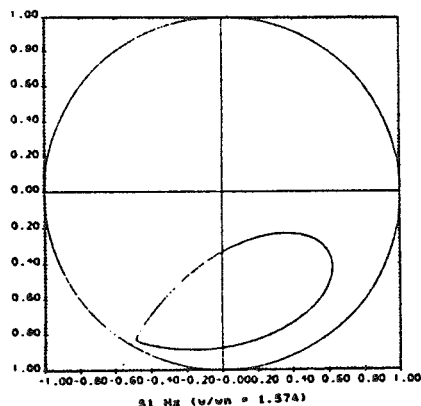
29 Hz ($u/u_n = 0.895$)



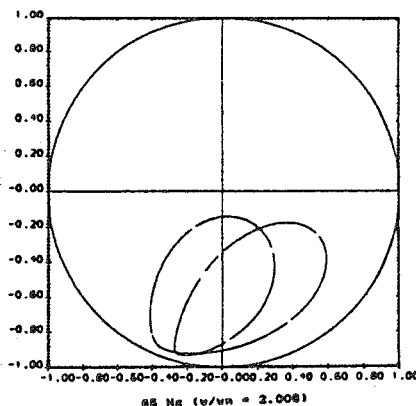
33 Hz ($u/u_n = 1.019$)



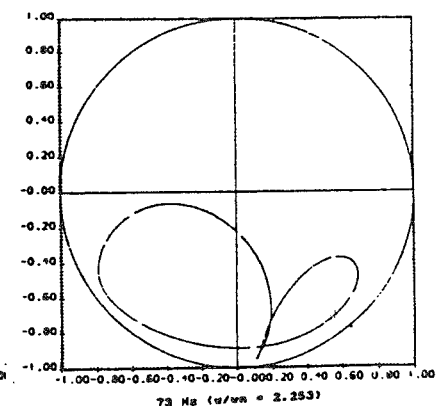
41 Hz ($u/u_n = 1.265$)



51 Hz ($u/u_n = 1.574$)

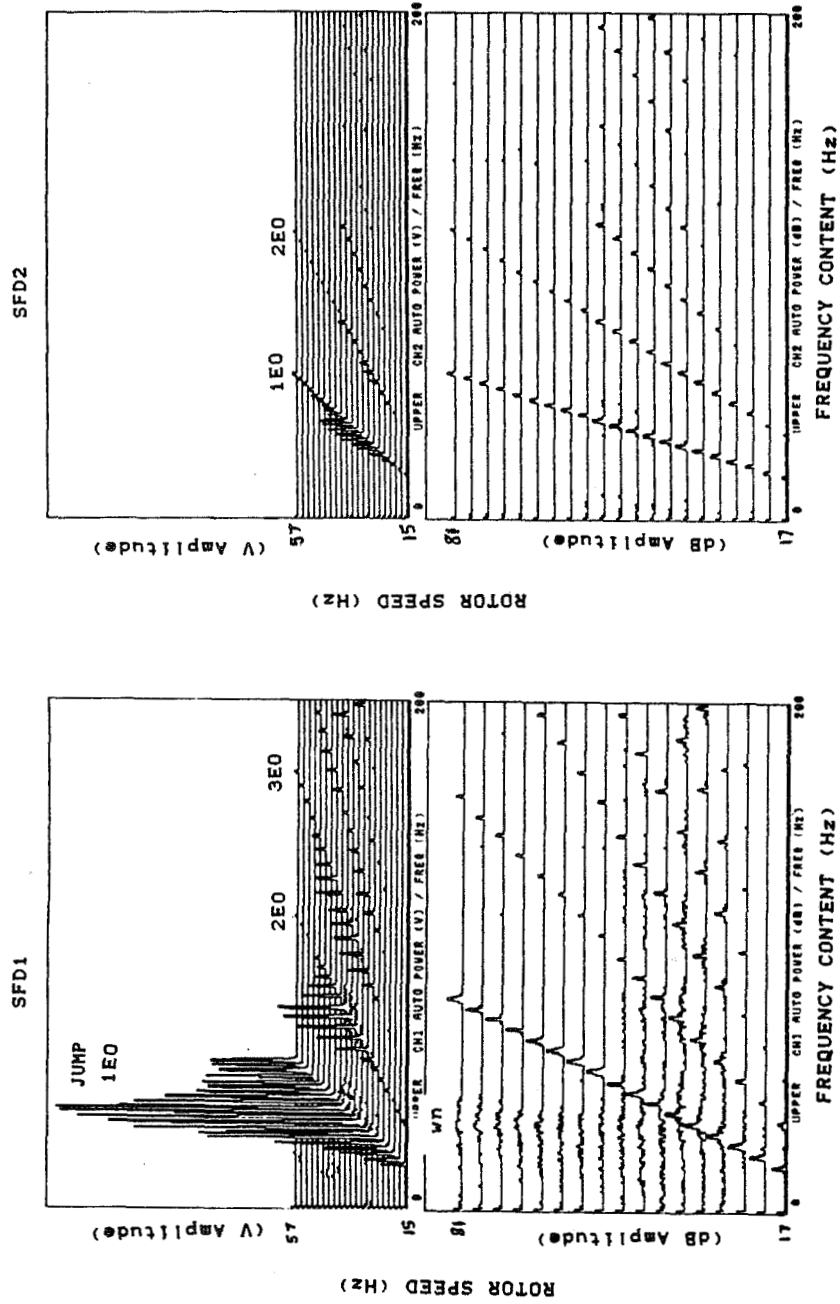


65 Hz ($u/u_n = 2.006$)



73 Hz ($u/u_n = 2.253$)

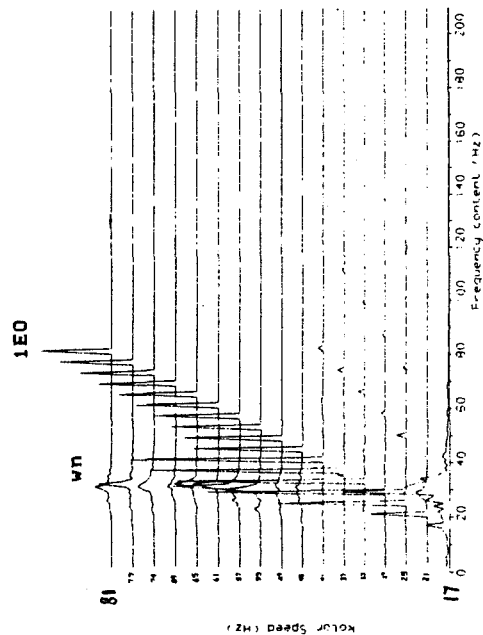
(d) SFD1 THEORETICAL ORBITS (Configuration 1b, $Q_{c2} = 0.490$, $P_{sup} = 2\text{psi}$, $E_{o1} = 0.8$)



(a)

Experimental Waterfall Diagram

A = 0.211200E -1
Qc2 = 0.610707E 0
Eo = 0.000000E 0
Psup = 0.200000E 1 (psi)
Pmin = -0.147000E 2 (psi)

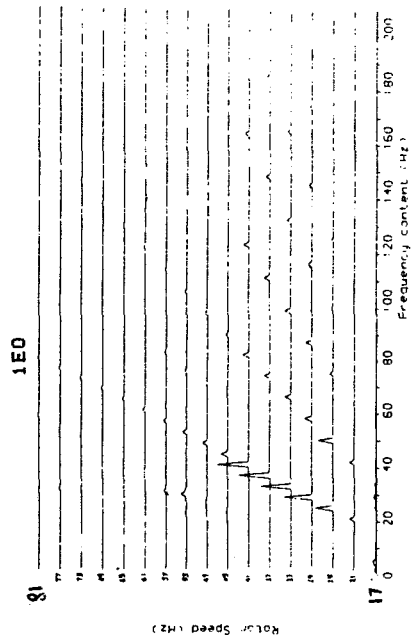


SFD1

(Linear Amplitude)

(b)

A = 0.401000E -1
Qc2 = 0.610707E 0
Eo = 0.100000E 1
Psup = 0.200000E 1 (psi)
Pmin = -0.147000E 2 (psi)



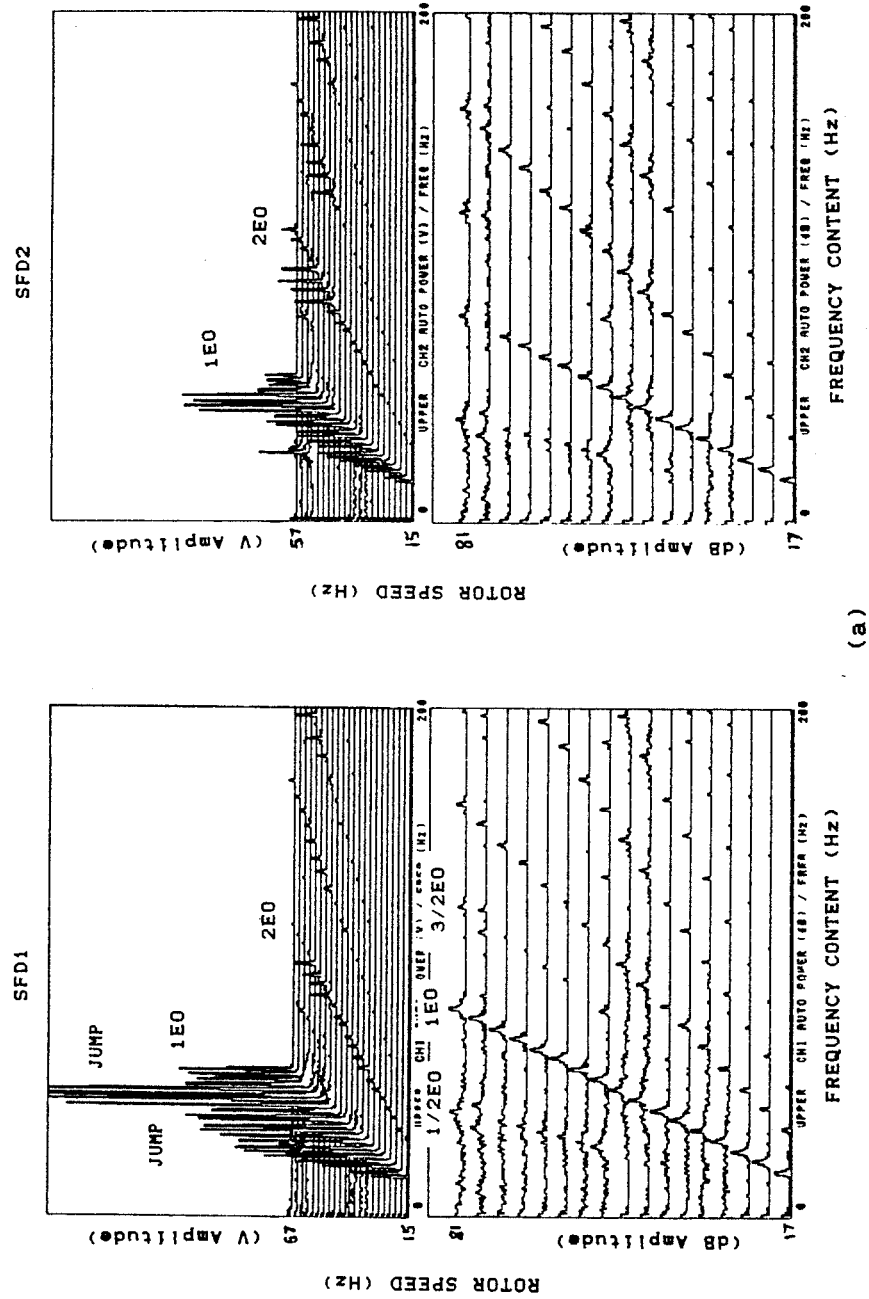
SFD2

(Linear Amplitude)

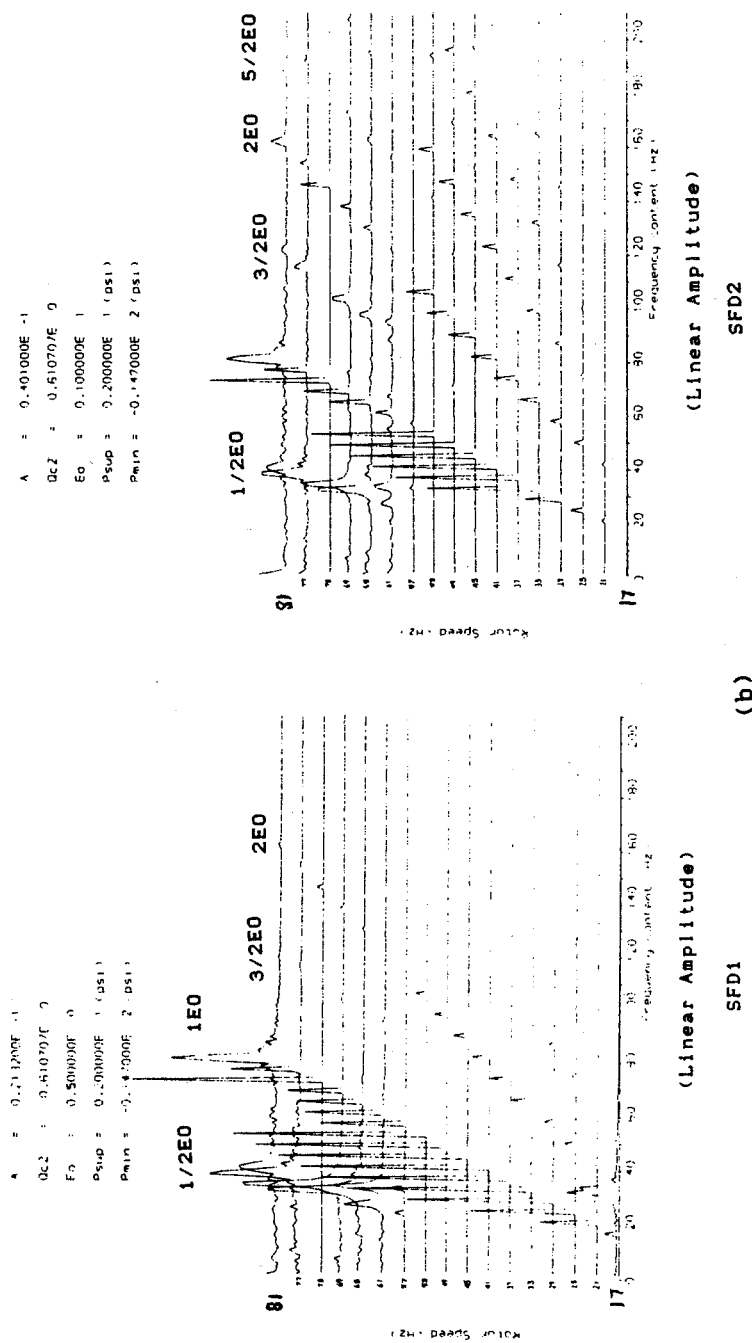
Theoretical Waterfall Diagram

Configuration 2a ($Q_{c2}=0.611$, $P_{sup}=2\text{psi}$, $E_o=0.0$)

Fig 7



Experimental Waterfall Diagram

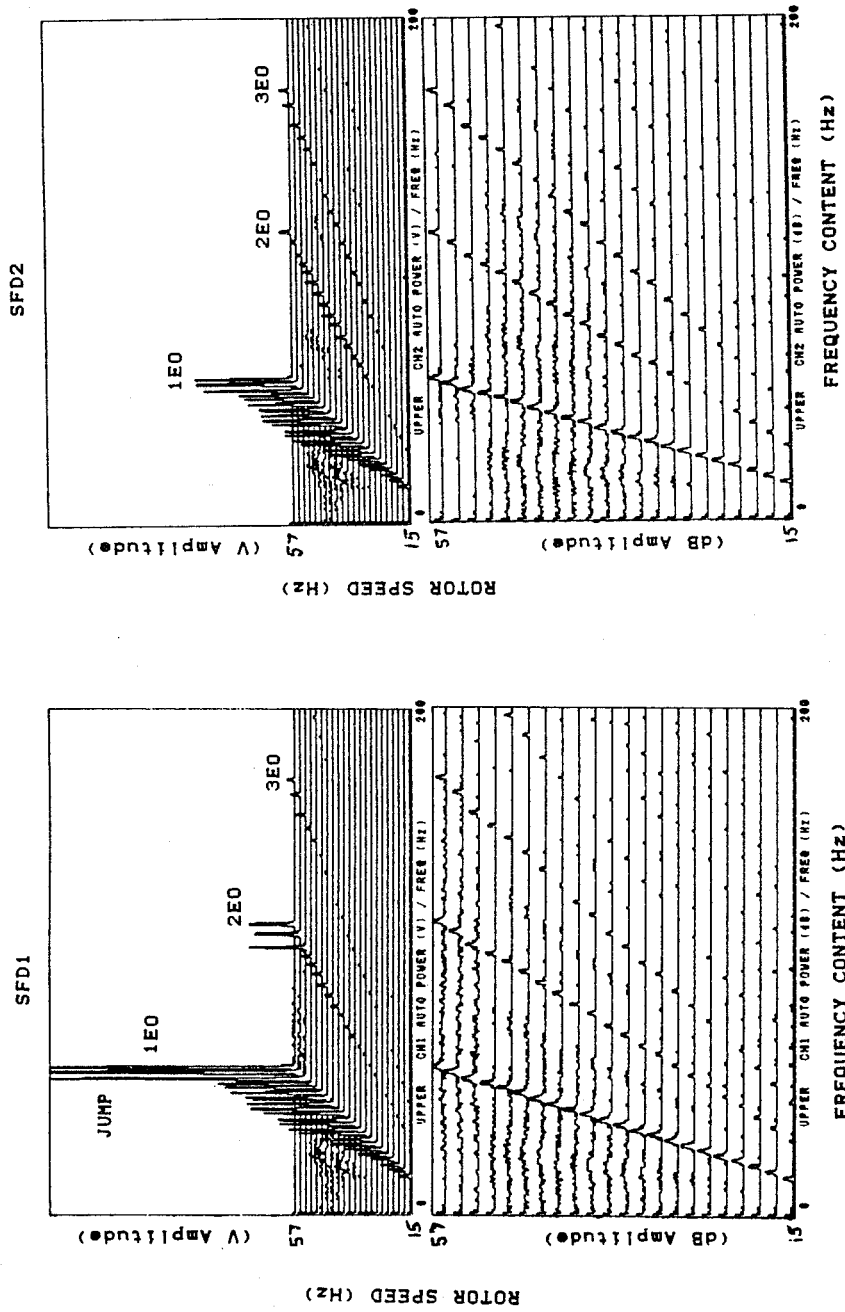


(b)

Theoretical Waterfall Diagram

Configuration 2a ($Qc_2=0.611$, $P_{sup}=2\text{psi}$, $E_0=0.5$)

Fig 8



(a)

Experimental Waterfall Diagram

45



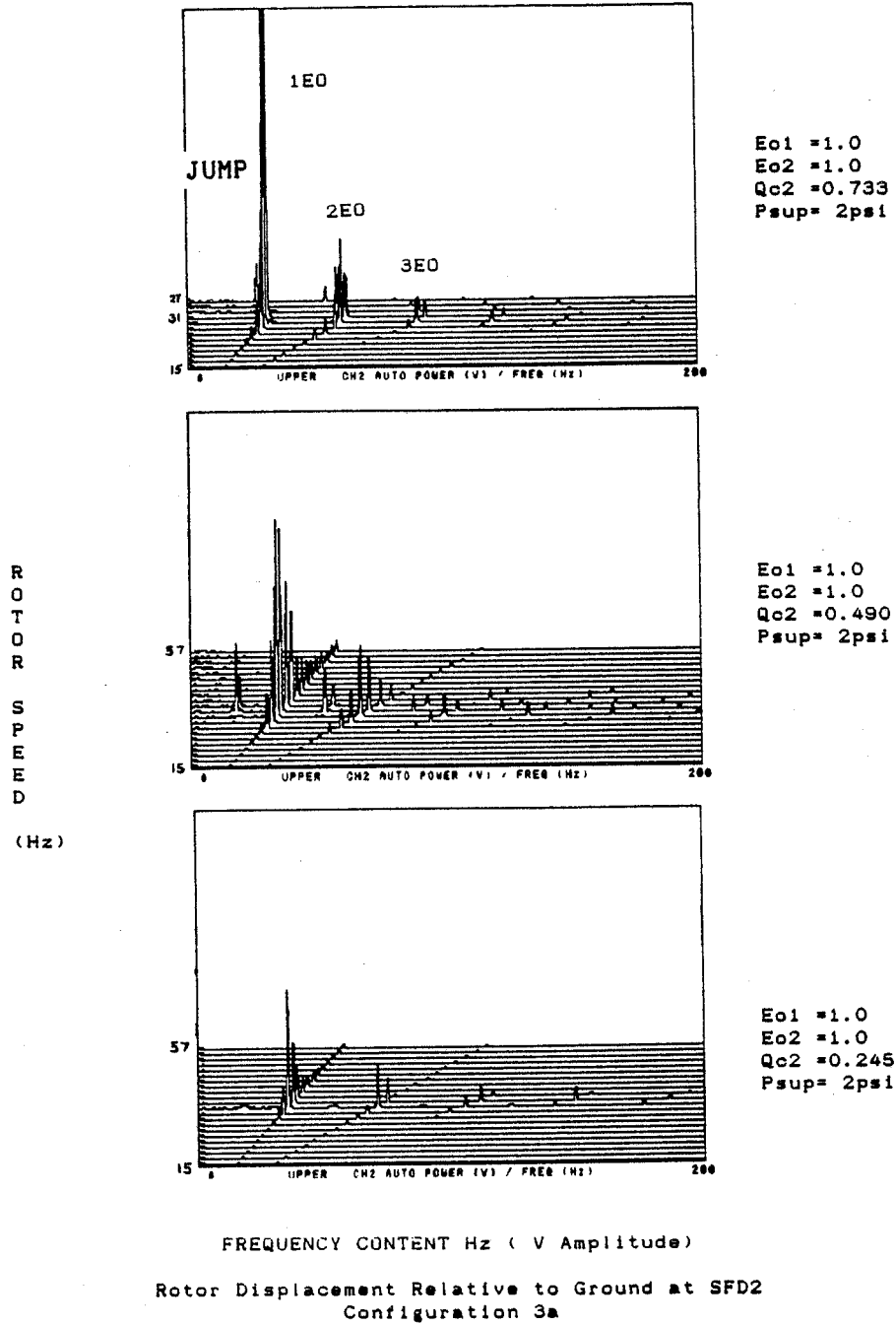
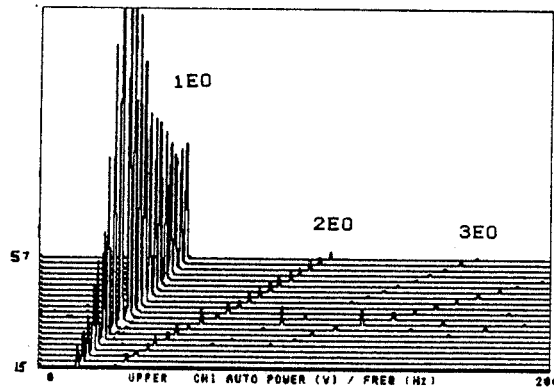


Fig 10

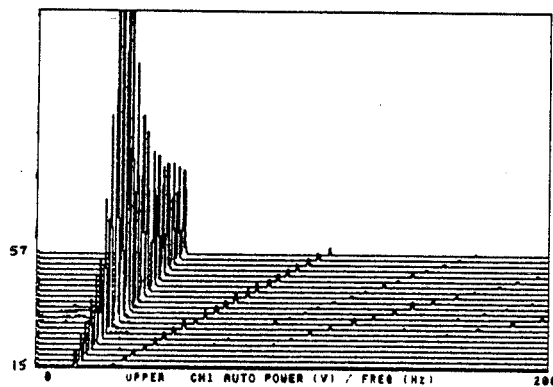
R
O
T
O
R

S
P
E
E
D

(Hz)



Eo1 =0.0
Eo2 =1.0
Qc2 =0.611
Psup= 2psi



Eo1 =0.0
Eo2 =1.0
Qc2 =0.490
Psup= 2psi

SFD1 FREQUENCY CONTENT Hz (V Amplitude)
Rotor Displacement Relative to Ground at SFD2
Configuration 3b

ORIGINAL PAGE IS
OF POOR QUALITY